Available online at www.sciencedirect.com

jmr&t Journal of Materials Research and Technology

journal homepage: www.elsevier.com/locate/jmrt

Original Article

Zirconia responses to edge chipping damage induced in conventional and ultrasonic vibration-assisted diamond machining

Afifah Z. Juri, Yanzhong Zhang, Andrei Kotousov, Ling Yin *

School of Mechanical Engineering, The University of Adelaide, Adelaide, SA, 5005, Australia

ARTICLE INFO

Article history:
Received 22 November 2020
Accepted 2 May 2021
Available online 7 May 2021

Keywords:
Edge chipping damage
Diamond machining
Microstructure
Ultrasonic vibration assistance
Zirconia

ABSTRACT

Machining-induced edge chipping damage represents a common challenge in ceramic applications. This paper reports on responses of zirconia materials with porous and dense microstructures to edge chipping damage induced in conventional and ultrasonic vibration-assisted diamond machining. The machining-induced damage was evaluated using optical and scanning electron microscopies. The results show that edge chipping damage produced in these processes was associated with brittle fracture and depends on the material microstructure and the vibration amplitude. Pre-sintered porous zirconia with a high brittleness index yielded significantly larger edge chipping damage than sintered dense zirconia with a low index in these processes. Ultrasonic machining at an optimal vibration amplitude minimized the scale of brittle fracture at the micro level, and thus significantly diminished edge chipping damage in zirconia materials with distinct microstructures. The investigation underpins the transition from conventional to ultrasonic vibration-assisted machining for manufacturing of ceramics to achieve better product quality.

1. Introduction

Zirconia is an attractive structural material widely applied in engineering and medicine due to its high strength and fracture toughness, low thermal conductivity, and good wear and corrosion resistance [1–3]. Excellent biocompatibility, aesthetic appearance, and optimal osseointegration has made this material very popular for dental applications [4–9]. However, zirconia's brittleness, poor manufacturability and susceptibility to machining-induced damage are main challenges and thus hinder its wider use.

Zirconia has porous and dense microstructures depending on sintering conditions and is subject to diamond machining to form precise shapes and sizes. Pre-sintered zirconia has a porous microstructure and low mechanical strength of 50–90 MPa [10], thus can be rapidly and economically machined using inexpensive and low stiffness tools [11–14]. However, sintering must be processed to densify its porous structure and increase its mechanical strength, which induces

* Corresponding author.
E-mail address: ling.yin@adelaide.edu.au (L. Yin).
https://doi.org/10.1016/j.jmrt.2021.05.005

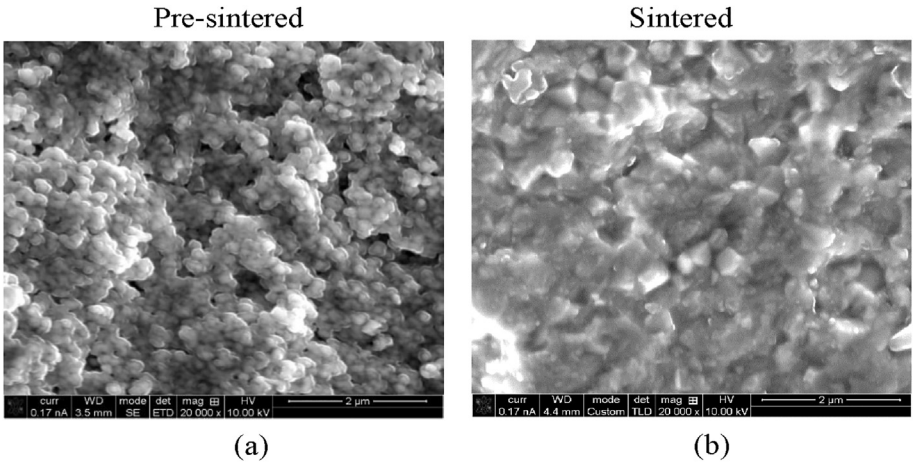

Fig. 1 – High magnification (20,000×) SEM micrographs revealing the microstructures of (a), fractured pre-sintered porous and (b), sintered dense zirconia materials.

approximately 20% bulk volume shrinkages [15,16], resulting in geometrical distortions for zirconia products. Thus, shrinkage compensations must be included in initial design as well as diamond machining, and polishing processes, making manufacturing processes more complex and less precise [17]. Sintered zirconia has a dense microstructure and high mechanical strength of 1100 ± 200 MPa [5,18], and can be machined for precise and accurate profiles using high-precision and high-stiffness tools [19], leading to high machining costs, low efficiency and severe wear of diamond tools [17].

Although zirconia is considered as "ceramic steel" [2], it is much more brittle than steels. As both porous and dense zirconia materials undergo diamond indentations and abrasion in fabrication processes, which unavoidably produce surface and subsurface damage to zirconia materials [20,21]. In particular, edge chipping damage representing the most severe type of mechanical damage. It has a significant impact on the mechanical functionality and reliability of zirconia products, such as zirconia crowns and bridges [22], and leads to fractures and failures of the products [23]. Therefore, machining-induced damage in pre-sintered porous and sintered dense zirconia materials has recently become a focal point of research related to zirconia applications [20,21,24]. In machining of pre-sintered porous zirconia, cooling and lubrication also affected the generation of subsurface edge chipping damage in the material [21]. However, the evaluation of the damage is yet to be investigated. In machining of sintered dense zirconia, subsurface damage and edge chipping of 15–44 μm deep in the material surfaces have been reported [25,26], which depends on machining parameters. In spite of the importance of machining processes for zirconia materials, the quantitative studies of machining-induced edge chipping damage in zirconia materials with distinct porous and dense microstructures has not been documented. As mentioned above, machining-induced surface and subsurface defects were found to significantly affect the strength [26,27], toughness [26], hardness [28], fatigue and reliability [29,30], fracture behavior [31] and wear performance [32] of zirconia products. The problem of damage mitigation/reduction can be addressed with non-conventional machining processes, such as ultrasonic vibration-assisted machining.

Ultrasonic vibration-assisted machining as one of the emerging machining techniques, is a process to assist conventional machining by adding ultrasonic vibration to the motion of a cutting tool tip to make discontinuous tool–workpiece interactions [33,34]. Ultrasonic machining has been used to machine hard steels and alloys [35–37] and brittle materials [38–42]. For brittle materials, ultrasonic machining of pre-sintered porous alumina has resulted in a significant edge chipping reduction from 680 ± 30 μm to 70 ± 10 μm in comparison with conventional machining [41]. For feldspar-containing glass ceramics, ultrasonic dental handpeice machining has reduced edge chipping by 65% [40]. Although these studies have provided insights into applications of ultrasonic machining for several materials, its potential to reduce edge chipping damage for brittle materials remains unclear and needs further investigation.

This paper aims to systematically study machining-induced edge chipping damage in zirconia materials with porous and dense microstructures by using conventional and ultrasonic vibration-assisted diamond milling processes. Optical and scanning electron microscopies were applied to characterize edge chipping damage depths and areas, and morphology features. Overall, the current research facilitates the development of a transition to new manufacturing processes to improve diamond machining for reliable zirconia products.

2. Experimental procedure

2.1. *Materials*

A cylindrical blank of translucent pre-sintered zirconia with 98.5 mm diameter and 14 mm thickness (ZENOSTAR Zr Translucent, Wieland Dental + Technik GmbH & Co. KG, Pforzheim, Germany) was selected for this study. This material is generally utilized for dental CAD/CAM systems to

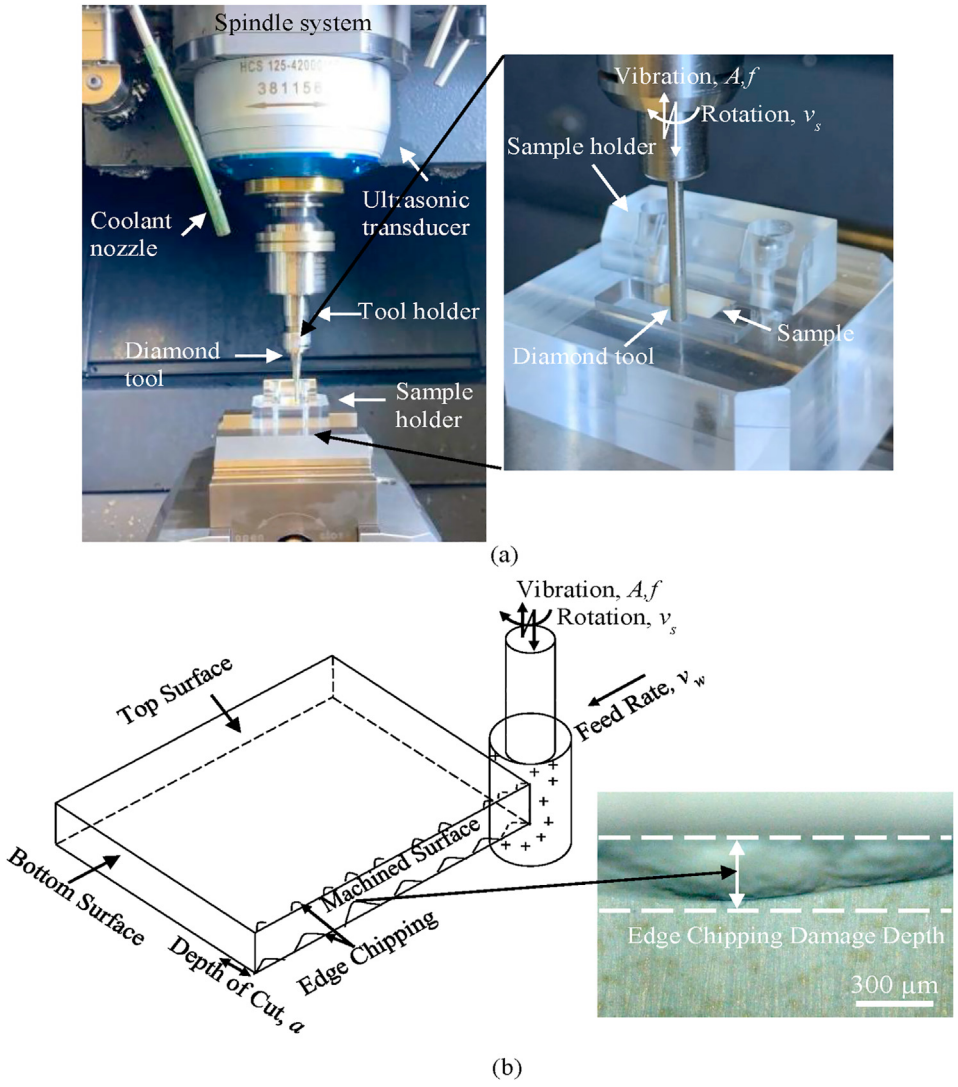

Fig. 2 – (a), Experimental setup for conventional and ultrasonic vibration-assisted diamond machining and (b), Sample-diamond tool movements for surface machining, machining-induced edge chipping damage on both top and bottom sample surfaces perpendicular to the machined surface, and edge chipping damage depth measurement.

produce zirconia crowns and bridges. It contains 91 wt% ZrO_2, 5 wt% Y_2O_3 as a stabilizer for retention of tetragonal grains at room temperature, 2 wt% HfO_2 as a binder for ZrO_2 powders [43] and 0.05 wt% Al_2O_3 as an agent to reduce the susceptibility of zirconia to low-temperature degradation [1,44]. Fig. 1a shows the microstructure of fractured pre-sintered zirconia using scanning electron microscopy (SEM, FEI Helios Nanolab 600, Thermo Fisher Scientific, USA). An interconnected and isolated porous microstructure of approximately 200 nm zirconia crystals was observed. The material porosity is in the range of 47.3–49.3 vol% [10]. The mechanical properties of the material include the Young's modulus E of 34 GPa [45], the hardness H of 1.5 GPa [45], the fracture toughness K_{IC} of 0.8 MPa $m^{1/2}$ [46] and flexural strength of 50–90 MPa [10].

Dense zirconia with a bulk density of more than 99% was achieved in a sintering process at a temperature of 1530 °C for 2 h using a digital dental furnace (Programat S1, Ivoclar Vivadent, Liechtenstein) at John Griffiths Dental Laboratory Australia. Fig. 1b shows the microstructures of fractured sintered zirconia using the SEM, revealing a highly dense and compacted microstructure of enlarged zirconia crystals of approximately 400 nm. The mechanical properties of the material include the Young's modulus E of 168 GPa [47], the hardness H of 13.2 GPa [47], the fracture toughness K_{IC} of 6 MPa $m^{1/2}$ [48], and the flexural strength of 1300 MPa [48].

Both pre-sintered porous and sintered dense zirconia samples were cut into rectangular blocks with dimensions of 10 × 10 × 2 mm using a diamond saw machine with a metal-bond 70 μm grit diamond disk of 450 μm thickness and 125 mm diameter (Struers Minitom, Denmark). The saw operated at a low speed with tap water as a coolant. Subsequently, top and bottom surfaces of 10 × 10 mm of each sample were polished using a polishing machine with 1200 grit silicon carbide grinding paper on a lap disc (Struers, Denmark) to parallel the two surfaces. Both surfaces were then progressively polished using 9–6 μm diamond pastes on wool cloth disks to achieve fine surfaces. Finally, all polished samples were cleaned using acetone. Top and bottom polished surfaces were observed

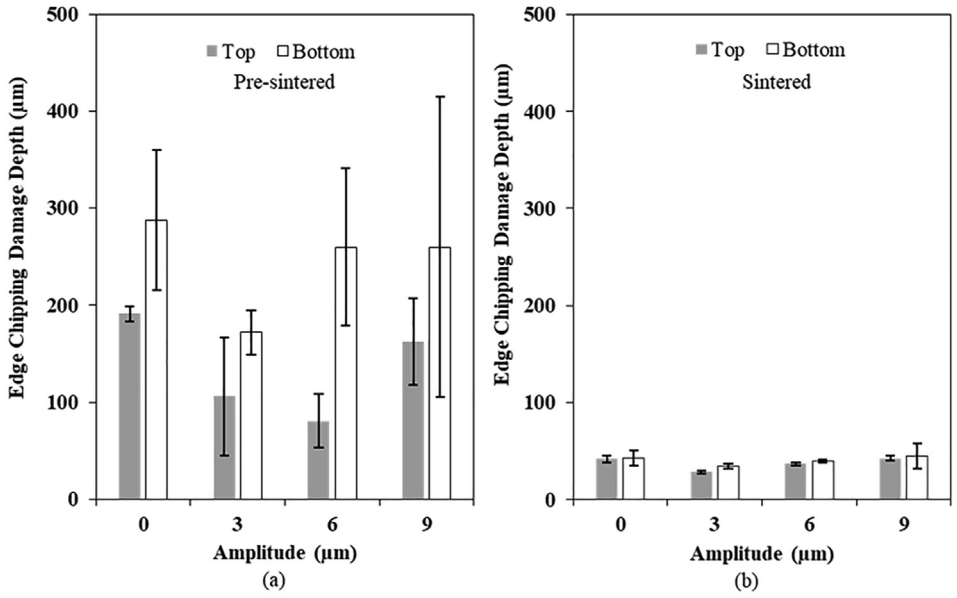

Fig. 3 – Edge chipping damage depths on top and bottom surfaces of (a), pre-sintered porous and (b), sintered dense zirconia materials produced by conventional and ultrasonic machining at different vibration amplitudes. Note that zero amplitude means conventional machining.

under optical microscopy (OM) to ensure all existing cracks or flaws were removed for subsequent machining processes.

2.2. *Conventional and ultrasonic vibration-assisted diamond milling*

Conventional and ultrasonic vibration-assisted diamond machining of zirconia materials were conducted using an ultrasonic high speed grinding/milling machine (Fig. 2) (Ultrasonic 20 Linear, DMG Mori Seiki CO., Ltd, Japan). The machine is a five-axis computer-controlled, high-speed, high-precision, high-efficiency grinding/milling unit integrated with an ultrasonic oscillation mechanism, enabling the maximum spindle rotational speed of 60,000 rpm for conventional machining and 50,000 rpm for ultrasonic vibration-assisted machining. The key machine structures shown in Fig. 2a includes a spindle system, an ultrasonic transducer, a tool holder installed with a diamond tool, a coolant nozzle, and a sample holder. The ultrasonic transducer driven by a piezoelectric actuator converts high-frequency electrical signals to high-frequency linear mechanical vibrations of the diamond tool along the spindle axis at 20–50 kHz frequencies and up to 10 μm vibration amplitudes. The cooling system supplies a coolant fluid into the machining zone for cooling and cleaning of machining debris.

Fig. 2b illustrates sample-diamond tool movements for surface machining, in which the diamond tool was initially positioned parallel to the 10 × 2 mm sample surface and then rotated at a machining speed of v_s along a 10 × 2 mm surface of the sample. A feed rate v_w parallel to the machined surface and a depth of cut a perpendicular to the machined surface were applied to remove a layer of material. In ultrasonic machining, the diamond tool also simultaneously rotated and axially vibrated at a frequency f and an amplitude A. The selected diamond tool had a cutting portion of 2 mm diameter and 4 mm length electroplated with 53 μm diamond grits (Schott, Diamantwerkzeuge GmbH, Germany). The selected conventional machining (i.e., vibration amplitude A = 0 as control) conditions for zirconia materials included a spindle speed v_s of 25,000 rpm, a feed rate v_w of 500 mm/min, and a depth of cut a of 50 μm. In addition to ultrasonic machining, vibration amplitudes of 3–9 μm at the harmonic frequency of the diamond tool 25 kHz were selected. During conventional and ultrasonic machining, a coolant (ECOCOOL 700 NBF (M), Fuchs Lubricants Australasia Pty Ltd, Australia) was injected to the sample-tool contact area at a pressure of 4 bars to prevent tool overheating and jamming, and to wash away debris.

2.3. *Characterization of edge chipping damage*

At each machining condition, 100 milling passes for each material were completed to obtain new machined surfaces. During machining, edge chipping damage was visible on both top and bottom polished surfaces perpendicular to the machined surface, as shown in Fig. 2b. After machining, all samples were cleaned using acetone.

Edge chipping damage in top and bottom surfaces illustrated in Fig. 2b, were first imaged using OM (ZEISS, Germany) installed with a camera and digital image processing software (AXIOvision software, ZEISS, Germany). On each top and bottom surface containing edge chipping damage, multiple images were continuously taken along a full edge length of 10 mm of a sample. Using Adobe Photoshop software, multiple images of edge chipping along the full length of each sample were merged. As shown in Fig. 2b, an edge chipping damage depth is defined as the vertical length between the damage bottom and the damage edge on a top or bottom surface. Under each machining condition, three largest edge chipping damage depths on each top or bottom surface were

measured to obtain the average and the standard deviation of the measurement [40] using AXIOvision software.

Based on the OM observation and measurement, ultrasonic machining at 3 μm vibration amplitude yielded least edge chipping damage to both materials. Then, top and bottom pre-sintered and sintered zirconia surfaces containing edge chipping damage produced in conventional and ultrasonic machining at 3 μm vibration amplitude were carbon-coated and examined using SEM (FEI Quanta 450 FEG ESEM, Thermo Fisher Scientific, USA).

A two-way analysis of variance (ANOVA) with replication at a 5% significance level was applied to examine the effects of edge surface locations and ultrasonic vibration amplitudes as independent variables on edge chipping damage depths. The paired *t*-test was also performed at 5% significance level to examine the influence of each material on edge chipping damage depths. The probability value, or the *p* value, was used to evaluate the significant results.

3. Results

3.1. *Edge chipping damage depths*

Fig. 3 shows edge chipping damage depths on top and bottom surfaces of pre-sintered porous and sintered dense zirconia materials produced in conventional (i.e., vibration amplitude = 0 as control) and ultrasonic machining at different vibration amplitudes. The data in Fig. 3 are also summarized in Table 1.

For pre-sintered porous zirconia in Fig. 3a, conventional machining produced edge chipping damage depths of 191 ± 8 μm and 288 ± 72 μm on top and bottom surfaces, respectively. In comparison, ultrasonic machining at 3 μm vibration amplitude reduced edge damage depths to 106 ± 61 μm by 45% and to 172 ± 23 μm by 40% on top and bottom surfaces, respectively. Table 2 shows the two-way ANOVA with replication for comparison of edge chipping damage depths in top and bottom surfaces in the porous material produced in conventional and ultrasonic machining at 3 μm vibration amplitude. It indicates that ultrasonic machining at such a vibration amplitude significantly reduced edge chipping damage depths than conventional machining (ANOVA, $p < 0.01$). It also shows that top and bottom edge chipping damage depths in both processes were significantly different (ANOVA, $p = 0.02 < 0.05$). Ultrasonic machining at 6 μm vibration amplitude, edge chipping damage depths decreased to 81 ± 27 μm by 58% and to 260 ± 81 μm by 9% on top and bottom surfaces in comparison with conventional machining, respectively. Ultrasonic machining at 9 μm vibration amplitude, edge chipping damage depths decreased to 162 ± 44 μm by 15% and to 260 ± 155 μm by 9% on top and bottom surfaces in comparison with conventional machining, respectively. Table 3 shows the two-way ANOVA with replication for comparison of edge chipping damage depths in top and bottom surfaces in pre-sintered porous zirconia produced in conventional and ultrasonic machining at 6 μm and 9 μm vibration amplitudes. It indicates that ultrasonic machining at such vibration amplitudes yielded insignificantly different edge chipping damage depths from conventional machining (ANOVA, $p = 0.37 > 0.05$). However, the top and bottom edge damage depths produced in these processes were significantly different (ANOVA, $p = 0.01 < 0.05$). All edge chipping damage on bottom surfaces in pre-sintered porous zirconia produced in conventional and ultrasonic machining were 1.5–3.3 times more severe than that on its top surfaces.

For sintered dense zirconia in Fig. 3b, conventional machining produced edge chipping damage depths of 42 ± 4 μm and 43 ± 8 μm on top and bottom surfaces, respectively. In comparison, ultrasonic machining at 3 μm vibration amplitude reduced edge damage depths to 28 ± 2 μm by 33% and to 35 ± 3 μm by 19% on top and bottom surfaces, respectively. Table 4 shows the two-way ANOVA with replication for comparison of edge chipping damage depths in top and bottom surfaces of sintered dense zirconia produced in conventional and ultrasonic machining at 3 μm vibration

Table 1 – Edge chipping damage depths (μm) in conventional and ultrasonic machining.

Ultrasonic vibration amplitude	Pre-sintered porous zirconia		Sintered dense zirconia	
	Top	Bottom	Top	Bottom
0 (Conventional)	191 ± 8	288 ± 72	42 ± 4	43 ± 8
3 μm	106 ± 61	172 ± 23	28 ± 2	35 ± 3
6 μm	81 ± 27	260 ± 81	37 ± 2	40 ± 2
9 μm	162 ± 44	260 ± 155	42 ± 2	44 ± 13

Table 2 – Two-way ANOVA with replication for comparison of edge chipping damage depths on top and bottom surfaces of pre-sintered porous zirconia produced in conventional and ultrasonic machining at 3 μm vibration amplitude.

Source of variation	Sum of square (SS)	DF	Mean sum of square (MS)	*F*-test	*p*-value	*F* crit
Edge location	19,983	1	19,983	8.38	0.02	5.32
Vibration amplitude	30,338	1	30,338	12.73	0.00	5.32
Interaction	719	1	719	0.30	0.60	5.32
Within	19,071	8	2384			
Total	70,111	11				

Table 3 – Two-way ANOVA with replication for comparison of edge chipping damage depths on top and bottom surfaces of pre-sintered porous zirconia produced in conventional and ultrasonic machining at 6 μm and 9 μm vibration amplitudes.

Source of variation	Sum of square (SS)	DF	Mean sum of square (MS)	*F*-test	*p*-value	*F* crit
Edge location	70,566	1	70,566	10.93	0.01	4.75
Vibration amplitude	14,167	2	7084	1.10	0.37	3.89
Interaction	6935	2	3468	0.54	0.60	3.89
Within	77,492	12	6458			
Total	169,162	17				

Table 4 – Two-way ANOVA with replication for comparison of edge chipping damage depths on top and bottom surfaces of sintered dense zirconia produced in conventional and ultrasonic machining at 3 μm vibration amplitude.

Source of variation	Sum of square (SS)	DF	Mean sum of square (MS)	F-test	p-value	F crit
Edge location	34	1	34	1.49	0.26	5.32
Vibration amplitude	373	1	373	16.52	0.00	5.32
Interaction	23	1	23	1.00	0.35	5.32
Within	181	8	23			
Total	610	11				

Table 5 – Two-way ANOVA with replication for comparison of edge chipping damage depths on top and bottom surfaces of sintered dense zirconia produced in conventional and ultrasonic machining at 6 μm and 9 μm vibration amplitudes.

Source of variation	Sum of square (SS)	DF	Mean sum of square (MS)	F-test	p-value	F crit
Edge location	17	1	17	0.40	0.54	4.75
Vibration amplitude	74	2	37	0.85	0.45	3.89
Interaction	6	2	3	0.07	0.93	3.89
Within	520	12	43			
Total	618	17				

amplitude. It indicates that ultrasonic machining at such a vibration amplitude significantly reduced edge chipping damage depths than conventional machining (ANOVA, $p < 0.01$). However, top and bottom edge chipping damage depths produced in both processes were insignificantly different (ANOVA, $p = 0.26 > 0.05$). Ultrasonic machining at 6 μm vibration amplitude, edge chipping damage depths decreased to 37 ± 2 μm by 12% and to 40 ± 2 μm by 7% on top and bottom surfaces in comparison with conventional machining, respectively. Ultrasonic machining at 9 μm vibration amplitude, edge chipping damage depths unchanged and slightly increased to 44 ± 13 μm by 5% on top and bottom surfaces in comparison with conventional machining, respectively. Table 5 shows the two-way ANOVA with replication for comparison of edge chipping damage depths in top and bottom surfaces of sintered dense zirconia produced in conventional and ultrasonic machining at 6 μm and 9 μm vibration amplitudes. It indicates that ultrasonic machining at such vibration amplitudes yielded insignificantly different edge chipping damage depths from conventional machining (ANOVA, $p = 0.45 > 0.05$). Further, the top and bottom edge damage depths produced in these processes were also insignificantly different (ANOVA, $p = 0.54 > 0.05$).

Comparing pre-sintered porous and sintered dense zirconia materials in Figs. 3a and b, conventional machining-induced edge chipping damage depths in the former top and bottom surfaces were 4.5 and 6.7 times those in the latter top and bottom surfaces, respectively. Ultrasonic machining-induced damage depths in the former top and bottom surfaces were 2.2–3.9 times and 4.9–5.9 times those in the latter top and bottom surfaces, respectively. Table 6 shows the t-test results for comparison of edge chipping damage depths in the two materials with two distinct microstructures produced in all machining conditions at all edge surface locations. It indicates that the material microstructure had a significant effect on edge chipping damage depths in the materials (t-test, $p < 0.01$).

3.2. SEM edge chipping damage morphology

Fig. 4 shows low-magnification (100×) SEM micrographs of edge chipping damage on top and bottom surfaces of pre-sintered porous and sintered dense zirconia materials produced by conventional and ultrasonic machining at 3 μm vibration amplitude. For pre-sintered porous zirconia shown in Fig. 4a–d, ultrasonic machining significantly reduced the maximum damage depth from 216 μm to 158 μm, by 27%, and from 381 μm to 171 μm, by 55%, on its top and bottom surfaces, respectively. For sintered dense zirconia shown in Figs. 4e–h, minimum conventional and ultrasonic machining-induced edge chipping damage can be observed on its top and bottom surfaces.

Fig. 5 shows higher magnification SEM micrographs of edge chipping damage features in pre-sintered porous zirconia produced by conventional and ultrasonic machining at 3 μm vibration amplitude. Fig. 5a reveals significant secondary edge chipping occurring in conventional machining, enhancing the original maximum chipping depth from 136 μm to 205 μm, by 51%. Fig. 5b reveals that ultrasonic machining produced smaller secondary edge chipping, increasing the original maximum chipping depth from 136 μm to 150 μm, by 10%. Both arrest lines and convex shell-like fractures in edge chipping scars are observed in conventional (Fig. 5c) and ultrasonic machining (Fig. 5d), respectively. Fig. 5e reveals a nearly identical conventional and ultrasonic machining-induced edge chipping damage morphology with irregular fractures and porous morphology.

Fig. 6 shows higher magnification SEM micrographs of edge chipping damage in top and bottom surfaces of sintered dense zirconia produced by conventional and ultrasonic machining

Table 6 – A paired t-test for edge chipping damage depths between pre-sintered porous and sintered dense zirconia materials produced in all machining conditions and at both top and bottom locations.

	Pre-sintered porous zirconia	Sintered dense zirconia
Mean	190	39
Variance	8917	49
Observations	24	24
Pooled Variance	4483	
Hypothesized Mean Difference	0	
Degree of freedom	46	
t Statistic	8	
p (T ≤ t) one-tail	0	
t Critical one-tail	2	
p (T ≤ t) two-tail	0	
t Critical two-tail	2	

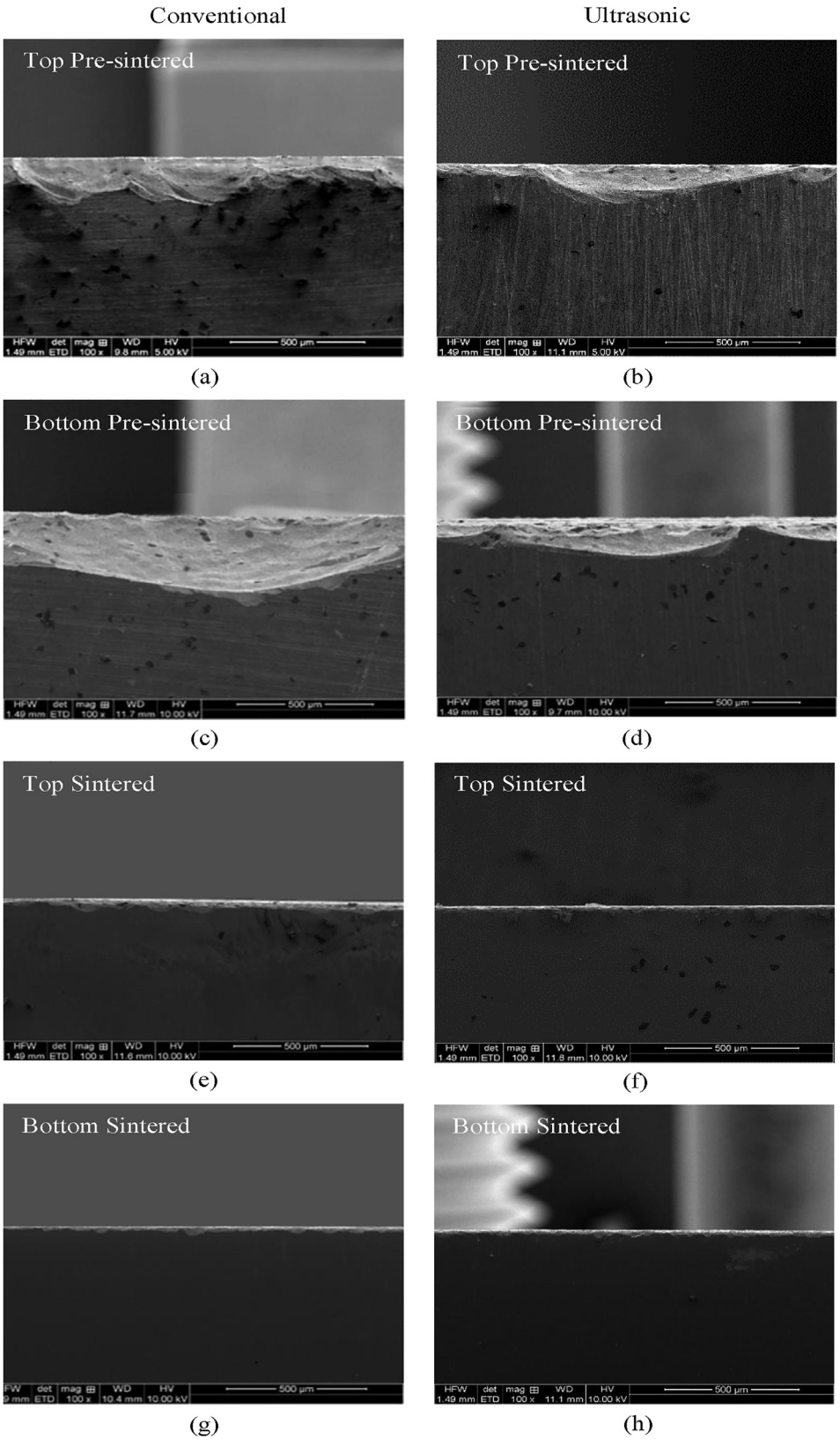

Fig. 4 – Low-magnification (100×) SEM micrographs of edge chipping damage in zirconia materials produced in conventional and ultrasonic machining at 3 μm vibration amplitude. (a), and (b), Top pre-sintered porous zirconia surfaces produced by conventional and ultrasonic machining, respectively; (c), and (d), Bottom pre-sintered porous zirconia surfaces produced by conventional and ultrasonic machining, respectively; (e), and (f), Top sintered dense zirconia surfaces produced by conventional and ultrasonic machining, respectively; (g), and (h), Bottom sintered dense zirconia surfaces produced by conventional and ultrasonic machining, respectively.

at 3 μm vibration amplitude. On top damaged surfaces shown in Figs. 6a and b, ultrasonic machining reduced the maximum damage depth from 41 μm to 29 μm, by 29%. On bottom damaged surfaces revealed in Figs. 6c and d, ultrasonic machining reduced the maximum damage depth from 45 μm to 36 μm, by 20%. Arrest lines and convex shell-like fractures were observed in these damaged scars. Fig. 6e reveals large cracks resulting from irregular fractures produced in conventional machining. Fig. 6f shows localized micro fractures created in ultrasonic machining, indicating reduced scales of edge chipping damage in the dense structure by ultrasonic machining.

4. Discussion

The results of this study have some intriguing implications concerning the application of ultrasonic vibration assistance to CAD/CAM diamond machining of pre-sintered porous and sintered dense zirconia materials. Particularly, edge chipping damage depths in the two materials with distinct microstructures in conventional and ultrasonic diamond machining have been compared in terms of maximum depths using OM and SEM, which are commonly used for damage studies at different resolutions [21,40]. Secondary chipping and detailed chipping morphologies and features, which were hardly visible using OM but clearly observed under SEM, contributed edge chipping damage degrees and reflect fracture mechanisms as shown in Figs. 4–6. All edge chipping damages cover damage areas. To reflect this areal feature, a Java-based image processing program (ImageJ, NIH Image, USA) was applied to measure edge chipping damage areas based on SEM micrographs in pre-sintered porous and sintered dense zirconia surfaces in Figs. 4 and 6. In the measurement, three repeats were conducted to obtain the means and standard deviations of the measured damage areas.

Fig. 7 shows the measurement of edge chipping damage areas in top and bottom surfaces of pre-sintered porous and sintered dense zirconia materials produced in conventional and ultrasonic machining at 3 μm vibration amplitude. Table 7 summarizes these damage area data, revealing that the ultrasonic machining-induced damage areas on top and bottom pre-sintered porous zirconia surfaces were reduced by 27% and 59%, respectively, whereas for sintered dense zirconia, the damage areas on top and bottom surfaces were decreased by 30% and 13%, respectively. A specific edge chipping damage area, i.e., edge chipping damage area per unit machining length ($\mu m^2/\mu m$), is used to compare maximum damage depths. Fig. 8 demonstrates specific edge chipping damage areas for top and bottom surfaces of pre-sintered porous and sintered dense zirconia materials produced in conventional and ultrasonic machining at 3 μm vibration amplitude. For pre-sintered porous zirconia, ultrasonic machining achieved significant reductions in specific edge chipping areas from 126 ± 5 $\mu m^2/\mu m$ to 92 ± 2 $\mu m^2/\mu m$, by 27%, and from 298 ± 2 $\mu m^2/\mu m$ to 121 ± 2 $\mu m^2/\mu m$, by 59%, on top and bottom surfaces, respectively. For sintered dense zirconia material, the corresponding reductions were obtained from 26 ± 1 $\mu m^2/\mu m$ to 19 ± 1 $\mu m^2/\mu m$, by 27%, and from 26 ± 1 $\mu m^2/\mu m$ to 22 ± 0 $\mu m^2/\mu m$, by 15%, on the latter top and bottom surfaces, respectively. This analysis reveals a similar trend to maximum edge chipping damage depths (Fig. 3) but reflects the true areal damage nature of edge chipping.

Figs. 3 and 4 show that pre-sintered porous zirconia yielded much more severe edge chipping damage than sintered dense zirconia in conventional and ultrasonic machining, indicating a significant material microstructure dependent nature of edge chipping damage formation as shown in Table 6 (t-test, $p < 0.01$). This is in agreement with studies on edge toughness studies of dental ceramics [49]. The material behavior affecting edge chipping damage is generally associated with its brittleness index expressed as [50]:

$$B = \frac{EH}{K_{IC}^2} \quad (1)$$

where H is the hardness, E is the Young's modulus, and K_{IC} is the fracture toughness. The brittleness indices of pre-sintered porous and sintered dense zirconia materials are calculated as 78 1/μ and 61 1/μ, respectively. A material with a higher brittleness index is more susceptible to brittle fracture. This means that pre-sintered porous zirconia is more susceptible to edge chipping damage than sintered dense zirconia in both conventional and ultrasonic machining, resulting in significantly deeper damage depths than those in sintered dense zirconia surfaces, as shown in Fig. 4. Sintering at high temperatures significantly influences zirconia microstructures by reducing porosity and increasing density, which, in turn, improve the mechanical properties [51–53]. Thus, sintered dense zirconia with much higher Young's modulus, hardness, fracture toughness and strength than its pre-sintered state, ultimately restrained edge chipping damage in conventional and ultrasonic machining. In addition, edge chipping occurs due to the existence of initial surface defects as crack origins to propagate under the action of machining forces, leading to fracture. Given the highly porous microstructure of pre-sintered zirconia (Fig. 5e), pores in the material also acted as initial surface defects, which easily nucleated, propagated and fractured to form edge chipping damage in diamond machining. In contrast, densely sintered zirconia with much less material defects revealed more resistance to edge chipping damage.

Ultrasonic machining at 3 μm vibration amplitude yielded least edge chipping depths for the two materials with distinct microstructures (ANOVA, $p < 0.05$) as shown in Figs. 3–6 and Tables 2 and 4, indicating the benefit of ultrasonic vibration assistance to diamond machining. Therefore, it is of great interest to elucidate the role of ultrasonic vibration in diamond machining and mechanisms to lead to less edge damage in terms of dynamic and kinematic analysis and finite element analysis (FEA) simulation. Firstly, from the dynamic and kinematic point of view, this study applied a one-dimensional ultrasonic vibration to the diamond tool axis direction, which was perpendicular to the feed direction, as shown in Fig. 9a. In conventional machining, diamond grains moved toward a zirconia surface at a rotational milling speed of v_s, a tool feed rate of v_w and a depth of cut of a to remove a layer of the material, as shown in Fig. 9b. In ultrasonic machining, an ultrasonic vibration with an amplitude of A and

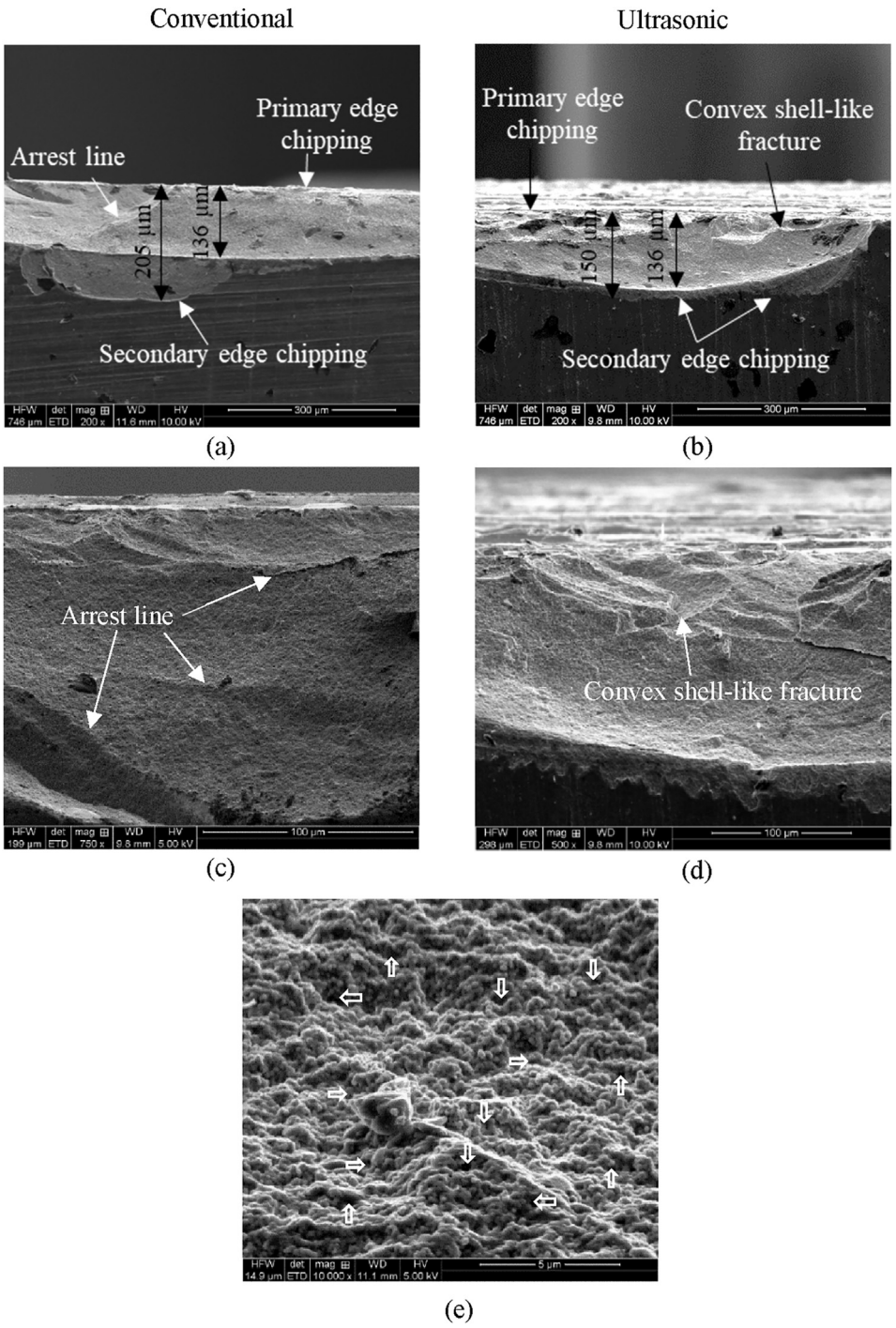

Fig. 5 – Higher-magnification SEM micrographs of edge chipping damage features in pre-sintered porous zirconia surfaces produced in conventional and ultrasonic machining at 3 μm vibration amplitude. (a), Significant secondary edge chipping damage below primary edge chipping damage produced in conventional machining; (b), Minor secondary edge chipping damage below primary edge chipping damage produced in ultrasonic machining; (c), Arrest lines in edge chipping damage produced in conventional machining; (d), Convex shell-like fractures in edge chipping damage produced in ultrasonic machining; (e), Nearly identical conventional and ultrasonic machining-induced edge chipping damage morphology of irregular fractures and porous microstructure. Arrows indicate pores.

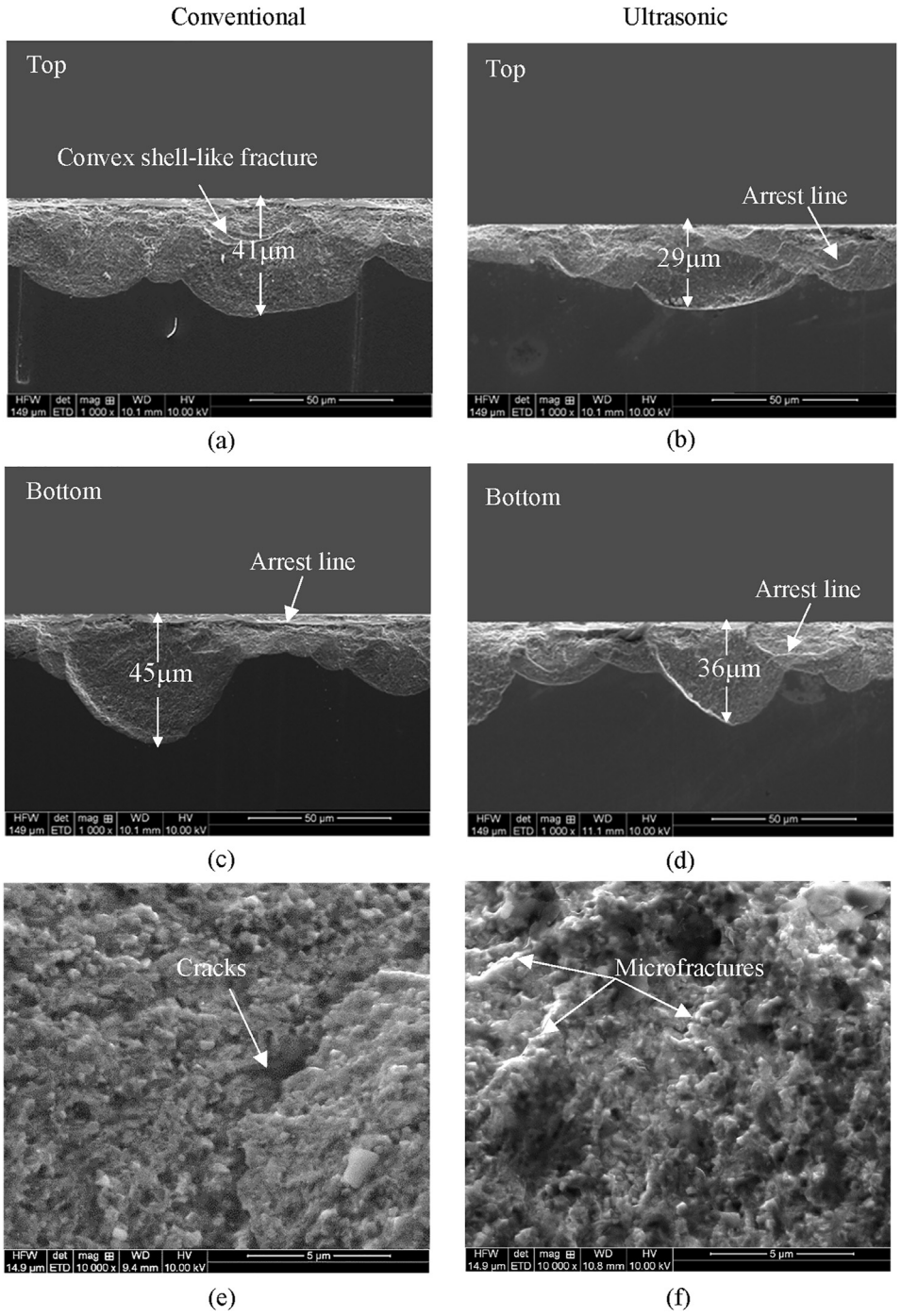

Fig. 6 – Higher-magnification SEM micrographs of edge chipping damage in top and bottom sintered dense zirconia surfaces produced by conventional and ultrasonic machining at 3 μm vibration amplitude. (a), and (b), Top surfaces with arrest lines and convex shell-like fracture produced by conventional and ultrasonic machining, respectively; (c), and (d), Bottom surfaces with arrest lines and convex shell-like fracture produced by conventional and ultrasonic machining, respectively; (e), Dense morphology and large cracks resulted from irregular fractures by conventional machining; and (f), Dense morphology and localized micro fracture produced by ultrasonic machining.

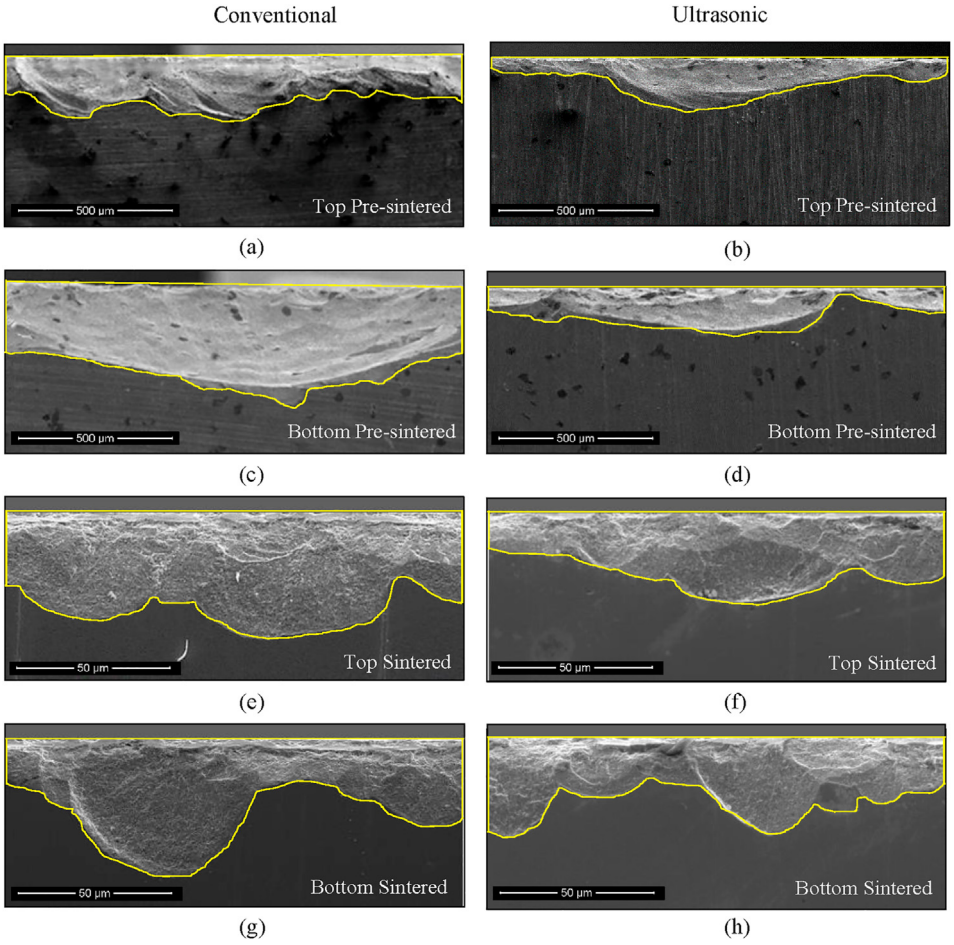

Fig. 7 – Measurement of edge chipping damage areas in zirconia materials induced by conventional and ultrasonic machining at 3 μm vibration amplitude. (a), and (b), Damages in top pre-sintered porous zirconia surfaces produced by conventional and ultrasonic machining, respectively; (c), and (d), Damages in bottom pre-sintered porous surfaces produced by conventional and ultrasonic machining, respectively; (e), and (f), Damages in top sintered dense zirconia surfaces produced by conventional and ultrasonic machining, respectively; (g), and (h), Damages in bottom sintered dense zirconia surfaces produced by conventional and ultrasonic machining, respectively.

a frequency of f added to conventional machining. The trajectory of a single diamond grain in conventional and ultrasonic machining can be parametrically described as [54]:

$$\begin{aligned} x &= v_w t + \frac{d}{2}\cos\left(\frac{2\pi v_s}{60}t\right) \\ y &= \frac{d}{2}\sin\left(\frac{2\pi v_s}{60}t\right) \\ z &= H_0 + A\sin(2\pi f t) \end{aligned} \quad (2)$$

Table 7 – Conventional and 3 μm vibration amplitude ultrasonic machining-induced damage areas (10^3 μm^2) on top and bottom surfaces of pre-sintered porous and sintered dense zirconia materials.

Ultrasonic vibration amplitude	Pre-sintered porous zirconia		Sintered dense zirconia	
	Top	Bottom	Top	Bottom
0 (Conventional)	185.3 ± 7.2	438.3 ± 3.2	3.9 ± 0.1	3.8 ± 0.1
3 μm	134.8 ± 3.0	178.1 ± 3.6	2.7 ± 0.1	3.3 ± 0.1

where d is the tool diameter, t is the cutting time and H_0 is the original height of the diamond grit. The cutting trajectory of a single diamond grain in conventional machining followed nearly a circular arc while the trajectory in ultrasonic machining traced a sinusoidal oscillation, as shown in Fig. 9c. Consequently, the relative motion relationship between the diamond tool and the zirconia surface in ultrasonic machining was changed to result in different material removal mechanisms from conventional machining.

Further, a mathematical model for ultrasonic vibration-assisted machining has identified an effective machining time for the period of diamond grain-workpiece contact with soda-lime glass as [55]:

$$t_{eff} = \frac{g}{2Af} \quad (3)$$

where t_{eff} is the effective cutting time, A is the vibration amplitude, f is the vibration frequency, and g is the diamond gain penetration depth. In ultrasonic vibration-assisted machining of brittle solids, each diamond grain may have indented and hammered a zirconia surface at a penetration

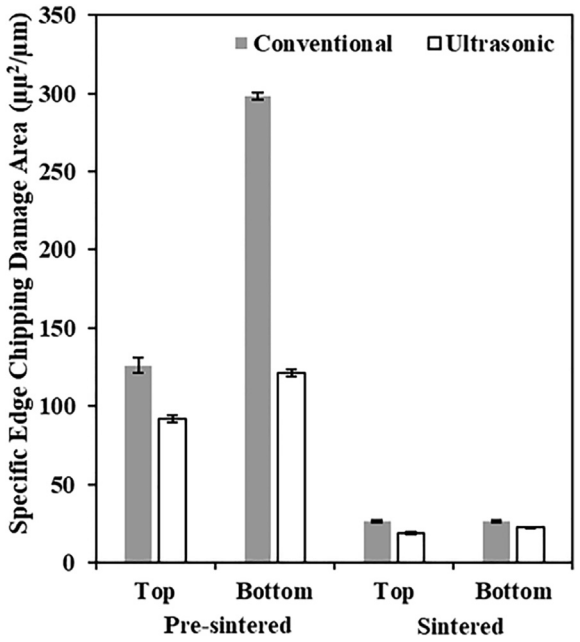

Fig. 8 – Specific edge chipping damage areas on top and bottom surfaces of zirconia materials produced in conventional and ultrasonic machining at 3 μm vibration amplitude.

depth for a period of effective machining time in a single ultrasonic vibration cycle. On the contrary, for conventional machining each diamond grain may have continuously contacted the zirconia surface. Accordingly, ultrasonic assisted machining has longer trajectory lengths than conventional machining, as shown in Fig. 9c.

In conventional machining, the interaction between the diamond tool and the zirconia surface was continuous. The interaction in ultrasonic machining was non-continuous due to sinusoidal oscillation trajectory-induced reciprocating separations between the diamond tool and the zirconia surface. This discontinuity was also confirmed in ultrasonic grinding of sintered zirconia using a CBN tool [56]. The high-frequency ultrasonic vibration inputting into the diamond grains allowed them to contact with the zirconia surface at shorter cutting times and to penetrate the surface at shallower depths during abrading. As a result of reciprocating separations and discontinuous interactions between the diamond tool and the zirconia surface in ultrasonic machining, contact frictions and machining forces might have been significantly reduced to yield shallower machining-induced edge chipping damage depths [40]. This finding is also supported by experimental results for alumina and silicon carbide ceramics [57–59].

Secondly, previous FEA simulation studies on edge chipping in rotary ultrasonic machining of alumina have predicted edge chipping initiation [60] based on the Withney-Nuismer point stress criterion [61]. The FEA model indicates that the scale of edge chipping damage in alumina was determined by controllable machining variables, i.e., machining speed, ultrasonic vibration amplitude, and feed rate [60]. However, the model has not compared the edge chipping damage in conventional and ultrasonic vibration-assisted machining. Efforts will be made to establish FEA modelling for comparison and prediction of edge chipping damage depths in both conventional and ultrasonic machining of pre-sintered porous and sintered dense zirconia materials.

Ultrasonic machining at 3 μm vibration amplitude might have altered material removal mechanisms for both zirconia materials. For pre-sintered porous zirconia, secondary edge chipping in conventional machining (Fig. 5a) was significantly larger than that in ultrasonic machining (Fig. 5b). For sintered dense zirconia, conventional machining induced large cracks on the chipping morphology (Fig. 6e) was not found in ultrasonic machining (Fig. 6f). These suggest that in ultrasonic machining, discontinuous interactions between diamond grains and zirconia surfaces might have contributed to reduced fracture scales for both materials in comparison to conventional machining. Fig. 10 shows removal mechanisms for conventional and ultrasonic machining processes, respectively. Conventional machining might have yielded larger scales of fractures and cracks as shown in Fig. 10a. In ultrasonic machining, microscale high-frequency ultrasonic vibrations applied to diamond grains might have impacted on the zirconia surface at higher active speeds and reduced forces, resulting in more microfractures and microcracks on the machined surface as shown in Fig. 10b. These distinct material removal mechanisms in conventional and ultrasonic machining may help to explain why ultrasonic machining at 3 μm vibration amplitude achieved least edge chipping damage for both zirconia materials. However, the fracture feature as the main material removal mode reflects the nature of conventional and ultrasonic machining both materials. Evidenced with arrest lines in Figs. 5 and 6, discontinuous crack propagations were observed in both materials produced by conventional and ultrasonic machining.

Higher vibration amplitudes of 6 μm and 9 μm might have scaled up microfracture and microcrack to larger fractures and cracks, leading to less or insignificant edge chipping damage reductions for both materials (ANOVA, $p > 0.05$) as shown in Fig. 3, Tables 3 and 5. Increased vibration amplitudes may have resulted in increased hammering actions of the diamond grains [62] on both material surfaces, inducing more chipping damage. This finding agrees with previous studies in which increased vibration amplitudes resulted in higher cutting forces and worse surface quality [63,64]. Hence, the selection of the ultrasonic vibration amplitude is crucial to improve the edge quality for zirconia materials and the vibration assistance at 3 μm vibration amplitude might be optimal for effective machining in this study.

Generally, ultrasonic vibration-assisted machining is performed at high frequency (typically 20 kHz) [65]. The current study applied 25 kHz, the harmonic frequency of the diamond tool determined by the machine. The application of such a harmonic frequency was recommended by the machine manufacturer and the studies on ultrasonic vibration-assisted machining of a carbon fiber reinforced polymer (CFRP) composite using the same machine [66]. Some optimality studies have predicted the increased material removal rates with the increased ultrasonic vibration frequency in the range of 10–40 kHz [67]. This paper has focused on the amplitude effect on the ultrasonic vibration-assisted machining of zirconia

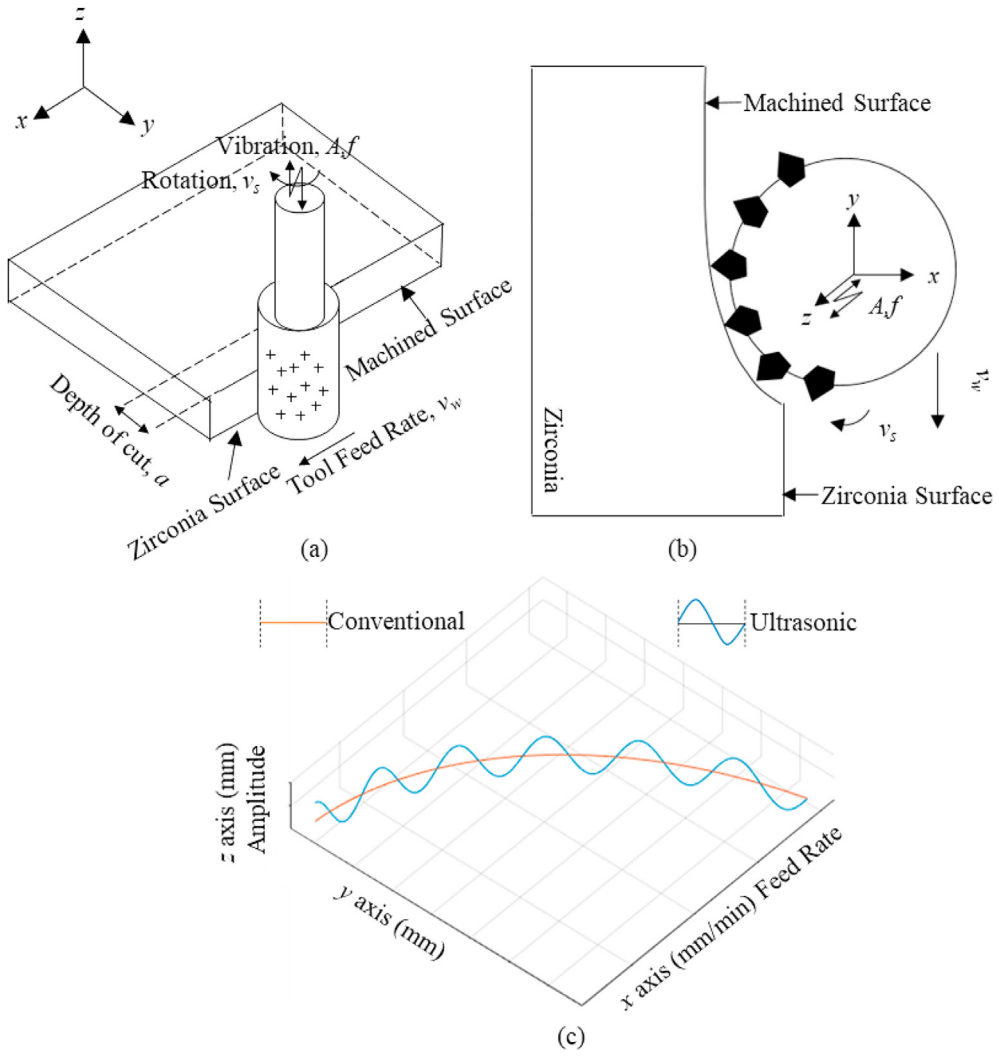

Fig. 9 – Illustration of conventional and ultrasonic machining processes. (a), 3D diamond machining; (b), 2D diamond grains-zirconia surface contact; and (c), Diamond grains trajectories in conventional and ultrasonic machining.

materials with distinct microstructure. The frequency effect in the machining processes will be studied in the future.

Although ultrasonic machining at 3 μm vibration amplitude significantly decreased edge chipping damage for both pre-sintered porous and sintered dense zirconia materials, the reduction rates for the former were significantly higher than the latter as shown in Figs. 3, 4 and 6. This may be attributed to the two materials with different machinability indices associated with their mechanical properties as follows [68]:

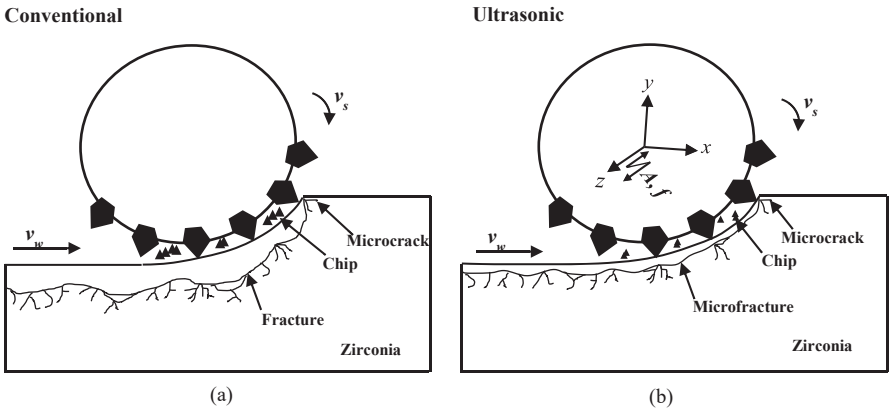

Fig. 10 – Illustration of removal mechanisms for (a), conventional and (b), ultrasonic machining.

$$M = \frac{\left(K_{IC}^{\frac{1}{2}} H^{\frac{9}{10}}\right)}{E^{2/5}} \quad (4)$$

where M is the machinability index, K_{IC} is the fracture toughness, H is the hardness and E is the elastic modulus. A higher machinability index indicates that the material is more difficult to machine. The machinability indices for pre-sintered porous and sintered dense zirconia materials are 4.3 MPa $m^{1/4}$ and 124.1 MPa $m^{1/4}$, respectively, indicating that the former is more machinable than the latter and the removal of edge chipping damage in the latter is much more difficult than the former. Therefore, any reduction in edge chipping damage in sintered dense zirconia would be very beneficial for post processing with respect to time and cost effectiveness.

Most previous edge chipping damage was observed or measured on single surfaces [40]. For the pre-sintered porous zirconia, edge chipping damage on bottom surfaces was found significantly larger than that on top surfaces in conventional and ultrasonic machining (ANOVA, $p < 0.05$) as shown in Figs. 3 and 4, and Tables 2 and 3. For the sintered dense zirconia, the damage scales on top and bottom surfaces in conventional and ultrasonic machining were similar (ANOVA, $p > 0.05$) as shown in Figs. 3 and 6, and Tables 4 and 5. In general, there are certain limitations in machining of brittle materials. Most studies have focused on fully dense solids with high hardness and Young's moduli, yielding higher cutting forces [69]. In conjunction with the low machine and tool stiffness, the forces produce deflections which negatively impact the dimensional accuracy of machined workpieces [69]. However, the machine used in this study (Fig. 2) is designed for high-precision machining of a wide range of materials from standard metals to difficult-to-cut materials of ceramics. Therefore, during machining of both zirconia materials, the machining-induced spindle-tool deflections was minimum.

Both pre-sintered porous and sintered dense zirconia materials were machined in the same machining conditions but significant different edge chipping depths on top and bottom surfaces were only measured for the former. Hence, the source of the difference may not favour the machining-induced spindle tool deflections in machining but may be attributed to the mechanical properties of the materials. The extreme low Young's modulus of 34 GPa [45] for the highly porous pre-sintered zirconia reflects its low resistance to the elastic deformation, which may have caused its machining-induced elastic deflections, leading to more severe edge chipping damage on bottom surfaces. The much higher Young's modulus of 168 GPa of the sintered dense zirconia [47] enables the material to have a higher resistance to the elastic deformation under machining, causing insignificant elastic defections. Thus, similar scales of machining-induced damages occurred on its top and bottom surfaces. Furthermore, little is known about machining-induced elastic deformation and deflections in soft, porous brittle solids, further studies are needed towards these issues.

5. Conclusions

This study reveals the microstructure-mechanical behavior-processing-induced edge damage relation in zirconia materials in conventional and ultrasonic vibration-assisted diamond machining. This research provides useful scientific fundamentals for the application of ultrasonic vibration assistance to diamond machining, enabling a potential improvement of conventional machining techniques for ceramic products. The following conclusions are drawn below:

(a) Pre-sintered porous zirconia with a high brittleness index yielded 4.5–6.7 and 2.2–5.9 times edge chipping damage than sintered dense zirconia with a low index in conventional and ultrasonic machining processes, respectively. The low elastic modulus of porous zirconia caused more chipping damage on bottom than top edges in both conventional and ultrasonic machining processes while such an edge location effect did not occur in the high elastic modulus of dense zirconia.
(b) Ultrasonic assisted machining at an optimal vibration amplitude of 3 μm achieved significant reductions in maximum edge chipping damage depths in pre-sintered porous and sintered dense zirconia materials by 40–45% and 19–33%, respectively.
(c) Caution must be taken in ultrasonic machining during which a suitable micro-scale vibration amplitude needs to be selected to enable the alteration of the material removal mechanisms for both materials from fracture to microscale fracture, leading to diminished subsurface edge chipping damage.
(d) A new concept of specific edge chipping area was proposed, which may be used as a precise assessment of edge chipping damage for all ceramics.

Declaration of Competing Interest

The authors declare that they have no known competing financial interests or personal relationships that could have appeared to influence the work reported in this paper.

Acknowledgments

The authors would like to thank Dr. Animesh Basak of the Adelaide Microscopy Centre and Mr. Evan Johnson of the Institute for Photonics & Advanced Sensing at the University of Adelaide (UoA) for experimental assistance. This work was supported by the UoA PhD Scholarship and seed grant in manufacturing and bio-manufacturing, and the Australian Research Council Grant No. DP200102300.

REFERENCES

[1] Denry I, Kelly JR. State of the art of zirconia for dental applications. Dent Mater 2008;24:299–307. https://doi.org/10.1016/j.dental.2007.05.007.

[2] Garvie RC, Hannink RH, Pascoe RT. Ceramic steel? Nature 1975;258:703–4. https://doi.org/10.1038/258703a0.

[3] Piconi C, Maccauro G. Zirconia as a ceramic biomaterial. Biomater 1999;20:1–25. https://doi.org/10.1016/S0142-9612(98)00010-6.

[4] Belli R, Wendler M, Ligny D, Cicconi MR, Petschelt A, Peterlik H, et al. Chairside CAD/CAM materials. Part 1: measurement of elastic constants and microstructural characterization. Dent Mater 2017;33:84–98. https://doi.org/10.1016/j.dental.2016.10.009.

[5] Schriwer C, Skjold A, Gjerdet NR, Øilo M. Monolithic zirconia dental crowns. Internal fit, margin quality, fracture mode and load at fracture. Dent Mater 2017;33:1012–20. https://doi.org/10.1016/j.dental.2017.06.009.

[6] Zhang Y, Lawn BR. Evaluating dental zirconia. Dent Mater 2019;35:15–23. https://doi.org/10.1016/j.dental.2018.08.291.

[7] Amarante JEV, Pereira MVS, De Souza GM, Pais Alves MFR, Simba BG, dos Santos C. Roughness and its effects on flexural strength of dental yttria-stabilized zirconia ceramics. Mater Sci Eng A 2019;739:149–57. https://doi.org/10.1016/j.msea.2018.10.027.

[8] Manicone PF, Rossi Iommetti P, Raffaelli L. An overview of zirconia ceramics: basic properties and clinical applications. J Dent 2007;35:819–26. https://doi.org/10.1016/j.jdent.2007.07.008.

[9] Schünemann FH, Galárraga-Vinueza ME, Magini R, Fredel M, Silva F, Souza JCM, et al. Zirconia surface modifications for implant dentistry. Mater Sci Eng C 2019;98:1294–305. https://doi.org/10.1016/j.msec.2019.01.062.

[10] Ritzberger C, Apel E, Höland W, Peschke A, Rheinberger VM. Properties and clinical application of three types of dental glass-ceramics and ceramics for CAD-CAM technologies. Mater 2010;3:3700–13. https://doi.org/10.3390/ma3063700.

[11] Lambert H, Durand JC, Jacquot B, Fages M. Dental biomaterials for chairside CAD/CAM: state of the art. J Adv Prosthodont 2017;9:486–95. https://doi.org/10.4047/jap.2017.9.6.486.

[12] Denry I. How and when does fabrication damage adversely affect the clinical performance of ceramic restorations? Dent Mater 2013;29:85–96. https://doi.org/10.1016/j.dental.2012.07.001.

[13] Meirowitz A, Bitterman Y, Levy S, Mijiritsky E, Dolev E. An in vitro evaluation of marginal fit zirconia crowns fabricated by a CAD-CAM dental laboratory and a milling center. BMC Oral Health 2019;19:1–6. https://doi.org/10.1186/s12903-019-0810-9.

[14] Fraga S, Amaral M, Bottino MA, Valandro LF, Kleverlaan CJ, May LG. Impact of machining on the flexural fatigue strength of glass and polycrystalline CAD/CAM ceramics. Dent Mater 2017;33:1286–97. https://doi.org/10.1016/j.dental.2017.07.019.

[15] Reich S, Wichmann M, Nkenke E, Proeschel P. Clinical fit of all-ceramic three-unit fixed partial dentures, generated with three different CAD/CAM systems. Eur J Oral Sci 2005;113:174–9. https://doi.org/10.1111/j.1600-0722.2004.00197.x.

[16] Sailer I, Fehér A, Filser F, Gauckler LJ, Lüthy H, Hämmerle CHF. Five-year clinical results of zirconia frameworks for posterior fixed partial dentures. Int J Prosthodont (IJP) 2007;20:383–8. https://pubmed.ncbi.nlm.nih.gov/17695869/.

[17] Miyazaki T, Nakamura T, Matsumura H, Ban S, Kobayashi T. Current status of zirconia restoration. J Prosthodont Res 2013;57:236–61. https://doi.org/10.1016/j.jpor.2013.09.001.

[18] Wendler M, Belli R, Petschelt A, Mevec D, Harrer W, Lube T, et al. Chairside CAD/CAM materials. Part 2: flexural strength testing. Dent Mater 2017;33:99–109. https://doi.org/10.1016/j.dental.2016.10.008.

[19] Abduo J, Lyons K, Swain M. Fit of zirconia fixed partial denture: a systematic review. J Oral Rehabil 2010;37:866–76. https://doi.org/10.1111/j.1365-2842.2010.02113.x.

[20] Denkena B, Breidenstein B, Busemann S, Lehr CM. Impact of hard machining on zirconia based ceramics for dental applications. Procedia CIRP 2017;65:248–52. https://doi.org/10.1016/j.procir.2017.04.055.

[21] Suya Prem Anand P, Arunachalam N, Vijayaraghavan L. Effect of grinding on subsurface modifications of pre-sintered zirconia under different cooling and lubrication conditions. J Mech Behav Biomed Mater 2018;86:122–30. https://doi.org/10.1016/j.jmbbm.2018.06.026.

[22] Schmitter M, Mueller D, Rues S. Chipping behavior of all-ceramic crowns with zirconia framework and CAD/CAM manufactured veneer. J Dent 2012;40:154–62. https://doi.org/10.1016/j.jdent.2011.12.007.

[23] Triwatana P, Nagaviroj N, Tulapornchai C. Clinical performance and failures of zirconia-based fixed partial dentures: a review literature. J Adv Prosthodont 2012;4:76–83. https://doi.org/10.4047/jap.2012.4.2.76.

[24] Alao AR, Stoll R, Song XF, Miyazaki T, Hotta Y, Shibata Y, et al. Surface quality of yttria-stabilized tetragonal zirconia polycrystal in CAD/CAM milling, sintering, polishing and sandblasting processes. J Mech Behav Biomed Mater 2017;65:102–16. https://doi.org/10.1016/j.jmbbm.2016.08.021.

[25] Luthardt RG, Holzhüter MS, Rudolph H, Herold V, Walter MH. CAD/CAM-machining effects on Y-TZP zirconia. Dent Mater 2004;20:655–62. https://doi.org/10.1016/j.dental.2003. 08.007.

[26] Xu HHK, Jahanmir S, Ives LK. Effect of grinding on strength of tetragonal zirconia and zirconia-toughened alumina. Mach Sci Technol 1997;1:49–66. https://doi.org/10.1080/10940349708945637.

[27] Guazzato M, Quach L, Albakry M, Swain MV. Influence of surface and heat treatments on the flexural strength of Y-TZP dental ceramic. J Dent 2005;3:9–18. https://doi.org/10.1016/j.jdent.2004.07.001.

[28] Anand PSP, Arunachalam N, Vijayaraghavan L. Study on grinding of pre-sintered zirconia using diamond wheel. Mater Manuf Process 2018;33:634–43. https://doi.org/10.1080/10426914.2017.1364761.

[29] Denry IL, Holloway JA. Microstructural and crystallographic surface changes after grinding zirconia-based dental ceramics. J Biomed Mater Res B Appl Biomater 2006;76:440–8. https://doi.org/10.1002/jbm.b.30382.

[30] Kosmač T, Oblak C, Jevnikar P, Funduk N, Marion L. The effect of surface grinding and sandblasting on flexural strength and reliability of Y-TZP zirconia ceramic. Dent Mater 1999;15:426–33. https://doi.org/10.1016/S0109-5641(99)00070-6.

[31] Passos SP, Linke B, Major PW, Nychka JA. The effect of air-abrasion and heat treatment on the fracture behavior of Y-TZP. Dent Mater 2015;31:1011–21. https://doi.org/10.1016/j.dental.2015.05.008.

[32] Mitov G, Heintze SD, Walz S, Woll K, Muecklich F, Pospiech P. Wear behavior of dental Y-TZP ceramic against natural enamel after different finishing procedures. Dent Mater 2012;28:909–18. https://doi.org/10.1016/j.dental.2012.04.010.

[33] Xu WX, Zhang LC. Ultrasonic vibration-assisted machining: principle, design and application. Adv Manuf 2015;3:173–92. https://doi.org/10.1007/s40436-015-0115-4.

[34] Yang Z, Zhu L, Zhang G, Ni C, Lin B. Review of ultrasonic vibration-assisted machining in advanced materials. Int J Mach Tool Manufact 2020;156:103594. https://doi.org/10.1016/j.ijmachtools.2020.103594.
[35] Chen S, Zou P, Tian Y, Duan J, Wang W. Study on modal analysis and chip breaking mechanism of Inconel 718 by ultrasonic vibration-assisted drilling. Int J Adv Manuf Technol 2019;105:177–91. https://doi.org/10.1007/s00170-019-04155-6.
[36] Goiogana M, Sarasua JA, Ramos JM. Ultrasonic assisted electrical discharge machining for high aspect ratio blind holes. Procedia CIRP 2018;68:81–5. https://doi.org/10.1016/j.procir.2 017.12.026.
[37] Lotfi M, Sajjady SA, Amini S. Wettability analysis of titanium alloy in 3D elliptical ultrasonic assisted turning. Int J Light Mater Manuf 2019;2:235–40. https://doi.org/10.1016/j.ijlmm.2019.05.001.
[38] Yang Z, Zhu L, Lin B, Zhang G, Ni C, Sui T. The grinding force modeling and experimental study of ZrO_2 ceramic materials in ultrasonic vibration assisted grinding. Ceram Int 2019;45:8873–89. https://doi.org/10.1016/j.ceramint.2019.01.216.
[39] Alkawaz M, Hafiz M, Kasim M, Izamshah R. Study of dental zirconia milling using rotary ultrasonic machining. Int J Eng Technol 2018;7:181–3. https://www.sciencepubco.com/index.php/%20IJET/article/view/22881.
[40] Song XF, Yang JJ, Ren HT, Lin B, Nakanishi Y, Yin L. Ultrasonic assisted high rotational speed diamond machining of dental glass ceramics. Int J Adv Manuf Technol 2018;96:387–99. https://doi.org/10.1007/s00170-017-1571-8.
[41] Tesfay HD, Xu Z, Li ZC. Ultrasonic vibration assisted grinding of bio-ceramic materials: an experimental study on edge chippings with hertzian indentation tests. Int J Adv Manuf Technol 2016;86:3483–94. https://doi.org/10.1007/s00170-015-8326-1.
[42] Bhosale SB, Pawade RS, Brahmankar PK. Effect of process parameters on MRR, TWR and surface topography in ultrasonic machining of alumina-zirconia ceramic composite. Ceram Int 2014;40:12831–6. https://doi.org/10.1016/j.ceramint.2014.04.137.
[43] Monaco C, Tucci A, Esposito L, Scotti R. Microstructural changes produced by abrading Y-TZP in pre-sintered and sintered conditions. J Dent 2013;41:121–6. https://doi.org/10.1016/j.jdent.2012.06.009.
[44] Hallmann L, Ulmer P, Reusser E, Louvel M, Hämmerle CHF. Effect of dopants and sintering temperature on microstructure and low temperature degradation of dental Y-TZP-zirconia. J Eur Ceram Soc 2012;32:4091–104. https://doi.org/10.1016/j.jeurceramsoc.2012.07.032.
[45] Alao AR, Yin L. Nano-scale mechanical properties and behavior of pre-sintered zirconia. J Mech Behav Biomed Mater 2014;36:21–31. https://doi.org/10.1016/j.jmbbm.2014.03.019.
[46] Alao AR, Yin L. Assessment of elasticity, plasticity and resistance to machining-induced damage of porous pre-sintered zirconia using nanoindentation techniques. J Mater Sci Technol 2016;32:402–10. https://doi.org/10.1016/j.jmst.2016.02.009.
[47] Alao AR, Yin L. Loading rate effect on the mechanical behavior of zirconia in nanoindentation. Mater Sci Eng A 2014;619:247–55. https://doi.org/10.1016/j.msea.2014.09.101.
[48] Sakoda S, Nakao N, Watanabe I. The effect of abrading and cutting instruments on machinability of dental ceramics. J Mater Sci Mater Med 2018;29:1–7. https://doi.org/10.1007/s10856-018-6031-y.
[49] Quinn J, Su L, Flanders L, Lloyd I. Edge toughness and material properties related to the machining of dental ceramics. Mach Sci Technol 2000;4:291–304. https://doi.org/10.1080/10940340008945711.
[50] Quinn JB, Quinn GD. Indentation brittleness of ceramics: a fresh approach. J Mater Sci 1997;32:4331–46. https://doi.org/10.1023/A:1018671823059.
[51] Inokoshi M, Zhang F, De MJ, Minakuchi S, Naert I, Vleugels J, et al. Influence of sintering conditions on low-temperature degradation of dental zirconia. Dent Mater 2014;30:669–78. https://doi.org/10.1016/j.dental.2014.03.005.
[52] Kim MJ, Ahn JS, Kim JH, Kim HY, Kim WC. Effects of the sintering conditions of dental zirconia ceramics on the grain size and translucency. J Adv Prosthodont 2013;5:161–6. https://doi.org/10.4047/jap.2013.5.2.161.
[53] Ruiz L, Readey MJ. Effect of heat treatment on grain size, phase assemblage, and mechanical properties of 3 mol% Y-TZP. J Am Ceram Soc 1996;79:2331–40. https://doi.org/10.1111/j.1151-2916.1996.tb08980.x.
[54] Xiao X, Zheng K, Liao W, Meng H. Study on cutting force model in ultrasonic vibration assisted side grinding of zirconia ceramics. Int J Mach Tool Manufact 2016;104:58–67. https://doi.org/10.1016/j.ijmachtools.2016.01.004.
[55] El-Taybany Y, El-Hofy H. Mathematical model for cutting force in ultrasonic-assisted milling of soda-lime glass. Int J Adv Manuf Technol 2019;103:3953–68. https://link.springer.com/article/10.1007/s00170-019-03399-6.
[56] Yang Z, Zhu L, Ni C, Ning J. Investigation of surface topography formation mechanism based on abrasive-workpiece contact rate model in tangential ultrasonic vibration-assisted CBN grinding of ZrO_2 ceramics. Int J Mech Sci 2019;155:66–82. https://doi.org/10.1016/j.ijmecsci.2019.02.031.
[57] Ahmed Y, Cong WL, Stanco MR, Xu ZG, Pei ZJ, Treadwell C, et al. Rotary ultrasonic machining of alumina dental ceramics: a preliminary experimental study on surface and subsurface damages. J Manuf Sci Eng Trans ASME 2012;134:064501. https://doi.org/10.1115/1.4007711.
[58] Li ZC, Cai LW, Pei ZJ, Treadwell C. Edge-chipping reduction in rotary ultrasonic machining of ceramics: finite element analysis and experimental verification. Int J Mach Tool Manufact 2006;46:1469–77. https://doi.org/10.1016/j.ijmachtools.2005.09.002.
[59] Zeng WM, Li ZC, Pei ZJ, Treadwell C. Experimental observation of tool wear in rotary ultrasonic machining of advanced ceramics. Int J Mach Tool Manufact 2005;45:1468–73. https://doi.org/10.1016/j.ijmachtools.2005.01.031.
[60] Jiao Y, Liu WJ, Pei ZJ, Xin XJ, Treadwell C. Study on edge chipping in rotatory ultrasonic machining of ceramics: an integration of designed experiments and finite element method analysis. Trans ASME J Manu Sci Eng 2005;127:752–8. https://doi.org/10.1115/1.2034511. 2005.
[61] Whitney JM, Nuismer RJ. Stress fracture criteria for laminated composites containing stress concentration. J Compos Mater 1974;8:253–65. https://journals.sagepub.com/doi/abs/10.1177/002199837400800303.
[62] Tsai MY, Chang CT, Ho JK. The machining of hard mold steel by ultrasonic assisted end milling. Appl Sci 2016;6:1–12. https://doi.org/10.3390/app6110373.
[63] Abdo BMA, Anwar S, El-Tamimi A. Machinability study of biolox forte ceramic by milling microchannels using rotary ultrasonic machining. J Manuf Process 2019;43:175–91. https://doi.org/10.1016/j.jmapro.2019.05.031.
[64] Li C, Zhang F, Meng B, Liu L, Rao X. Material removal mechanism and grinding force modelling of ultrasonic vibration assisted grinding for SiC ceramics. Ceram Int 2017;43:2981–93. https://doi.org/10.1016/j.ceramint.2016.11.066.

[65] Liu DF, Cong WL, Pei ZJ, Tang YJ, Tang. A cutting force model for rotary ultrasonic machining of brittle materials. Int J Mach Tool Manufact 2012;52:77–84. https://doi.org/10.1016/j.ijmachtools.2011.09.006.

[66] Kuruc M, Necpal M, Vopát T, Šimna V, Peterka J. Influence of ultrasonic assistance on delamination during machining of CFRP composite. In: Majstorovic V, Jakovljevic Z, editors. Proceedings of 5th international conference on advanced manufacturing engineering and technologies. Switzerland: Springer; 2017. p. 443–50. https://link.springer.com/chapter/10.1007/978-3-319-56430-2_33.

[67] Rao RV, Pawar PJ, Davim JP. Parameter optimization of ultrasonic machining process using nontraditional optimization algorithms. Mater Manuf Process 2010;25:1120–30. https://doi.org/10.1080/10426914.2010.489788.

[68] Song XF, Ren HT, Yin L. Machinability of lithium disilicate glass ceramic in in vitro dental diamond bur adjusting process. J Mech Behav Biomed Mater 2016;53:78–92. https://doi.org/10.1016/j.jmbbm.2015.08.003.

[69] Malkin S, Hwang TW. Grinding mechanisms for ceramics. CIRP Ann 1996;45:569–80. https://doi.org/10.1016/S0007-8506(07)60511-3.